A hybrid injectable hydrogel from hyperbranched PEG macromer as a stem cell delivery and retention platform for diabetic wound healing

Xu, Qian; A, Sigen; Gao, Yongsheng; Guo, Linru; Creagh-Flynn, Jack; Zhou, Dezhong; Greiser, Udo; Dong, Yixiao; Wang, Fadang; Tai, Hongyun; Liu, Wenguang; Wang, Wei; Wang, Wenxin

Acta Biomaterialia

DOI:
10.1016/j.actbio.2018.05.039

Published: 15/07/2018

Peer reviewed version

A hybrid injectable hydrogel from hyperbranched PEG macromer as a stem cell delivery and retention platform for diabetic wound healing

Qian Xu[a,†], Sigen A[a,†], Yongsheng Gao[a], Linru Guo[b], Jack Creagh-Flynn[a], Dezhong Zhou[a], Udo Greiser[a], Yixiao Dong[a], Fagang Wang[c], Hongyun Tai[d], Wenguang Liu[b], Wei Wang[b,*], & Wenxin Wang[a,*]

a. Charles Institute of Dermatology, School of Medicine, University College Dublin, Dublin 4, Ireland.
b. School of Materials Science and Engineering, Tianjin Key Laboratory of Composite and Functional Materials, Tianjin University, Tianjin 300350, China.
c. Department of Burn & Plastic Surgery, Shandong Provincial Hospital Affiliated to Shandong University, Jinan 250001, China.
d. School of Chemistry, Bangor University, Bangor, Gwynedd LL57 2DG, UK

† These two authors contributed equally to this work.
* Corresponding authors:
E-mail: Dr. Wei Wang, email: wwgfz@tju.edu.cn;
Prof. Wenxin Wang, email: wenxin.wang@ucd.ie.

Keywords: diabetic wound healing, injectable hydrogels, hyperbranched polymers, stem cells, *in situ* RAFT

Abstract: The injectable hydrogel with desirable biocompatibility and tunable properties can improve the efficacy of stem cell-based therapy. However, the development of injectable hydrogel remains a great challenge due to the restriction of crosslinking efficiency, mechanical properties, and potential toxicity. Here, we report that a new injectable hydrogel system were fabricated from hyperbranched multi-acrylated poly(ethylene glycol) macromers (HP-PEGs) and thiolated hyaluronic acid (HA-SH) and used as a stem cell delivery and retention platform. The new HP-PEGs were synthesized *via in situ* reversible addition fragmentation chain transfer (RAFT) polymerization using an FDA approved anti-alcoholic drug - Disulfiram (DS) as the RAFT agent precursor. HP-PEGs can form injectable hydrogels with HA-SH

rapidly *via* thiol-ene click reaction under physiological conditions. The hydrogels exhibited stable mechanical properties, non-swelling and anti-fouling properties. Hydrogels encapsulating adipose-derived stem cells (ADSCs) have demonstrated promising regenerative capabilities such as the maintenance of ADSCs' stemness and secretion abilities. The ADSCs embedded hydrogels were tested on the treatment of diabetic wound in a diabetic murine animal model, showing enhanced wound healing.

1. Introduction

Diabetic wounds are a severe complication of diabetes that aggravates the patient's condition, and affects a dramatically increasing population.[1] In view of the specific pathophysiological abnormalities of the wound environment including prolonged inflammation, vascular problems, inhibited re-epithelialization, a major failure has been seen with single treatment or FDA approved therapy devices.[2] Therefore, a combined therapeutic approach using advanced technologies that alleviates the deleterious pathological factors is of great interest. There is a great promise for stem cell-based treatment for diabetic wounds that has been reported over the past decade.[3] However, the hostile wound environment minimizes the retention and survival of stem cells, which significantly limits the clinical translation of stem cell therapy. To maintain and protect the stem cells that have been delivered onto the harsh diabetic environment, hydrogel systems have been explored to improve the engraftment of transplanted stem cells for diabetic wound repair.[4] Among them, *in situ* formed injectable hydrogel system has attracted much attention for wound healing application in recent years.[5–7] The injectable hydrogel can be easily applied on any irregular

shape during hydrogel formation without using the complex mould,[8–10] and possess the advantages of easy administration, efficient cell encapsulation, minimal invasion, and enhanced patient compliance,[11] making them attractive for various biomedical applications. The components of injectable hydrogels range from natural (*e.g.* hyaluronic acid, chitosan, alginate, collagen, gelatin) to synthetic (*e.g.* poly(ethylene glycol), polyacrylamide, Poly(Lactide-co-Glycolide)) materials.[4] Naturally derived hydrogels have been frequently used in tissue engineering, as the components have the same or similar properties to the natural extracellular matrix (ECM).[12] However, these naturally derived biomaterials always show large heterogeneity in structure, poor stability and mechanical performance as well as relatively high cost.[13] Synthetic hydrogels are appealing for tissue engineering and regeneration as their properties are tunable, reproducible, and much easier to pre-design in order to meet numerous of specific requirements.[12] Although there have been various synthetic injectable hydrogels reported for wound healing application, a majority of the reported hydrogels suffer from potential toxicity, less biological cues and unsuitable mechanical properties, etc. which prevent the successful clinical translation of synthetic hydrogels.[14,15] Therefore, a well-designed *in situ* formed injectable hydrogel system that combines a well-constructed synthetic polymer with a properly selected naturally derived biopolymer could be an appropriate consideration to create improved materials to achieve an effective healing process.

Among numerous synthetic biomaterials, poly(ethylene glycol) (PEG) and its derivatives have been extensively used for fabrication of biocompatible hydrogels for

cell culture scaffolds[16] and tissue engineering.[17] However, the conventional linear and/or multi-armed star PEG (4-armed or 8-armed) based materials are suffering from their low functional group density, which largely restricts their reaction efficiency. One solution is to construct PEG materials with highly branched structures. As one of the classical approaches to synthesize branched polymers, 'Strathclyde route' is using free radical polymerization of mono-vinyl monomers with a small amount of divinyl crosslinkers.[18] However, the polymers produced by such an approach still possess limited pendent vinyl groups, which make them not ideal candidates as the crosslinkers to form injectable hydrogels. To overcome this drawback, Wang *et al.* proposed a kinetically controlled strategy to polymerize the multi-vinyl monomers.[19–24] PEG based hyperbranched polymers with high branching degree and pendent vinyl density were successfully achieved.[25–28] The high content of pendent vinyl groups endows them the ability to generate *in situ* injectable hydrogel systems rapidly. However, there is still one significant limitation on the previous studies which used atom transfer radical polymerization (ATRP) requiring potential toxic copper catalysts.

To address this issue, reversible addition fragmentation chain transfer (RAFT) polymerization has been used to synthesize PEG polymers without using toxic metal catalysts.[6,29] While, the most significant challenges in RAFT polymerization are the complicated synthesis procedure for RAFT agents, which needs to use noxious and toxic organic reagents (carbon disulfide or iodine), and the subsequent time-consuming reaction and purification steps.[30,31] Wang *et al.* explored one-pot

in situ RAFT polymerization of PEG-based monomethacrylate and dimethacrylate monomers by using bis(thiobenzoyl) disulfide as a precursor of RAFT agent and a well-controlled polymerization was obtained.[32] Inspired by this work, another chemical disulfiram (DS or tetraethylthiuram disulfide, as shown in Figure 1), was hypothesized that it can potentially be utilized to perform the *in situ* RAFT polymerization. This was successfully verified in our recent work, where a DS-poly(ethylene glycol) methyl ether acrylate (DS-PEGMEA) was synthesized *via* RAFT polymerization utilizing DS as the RAFT precursor.[33] One advantage of using DS as the RAFT agent precursor is the relatively low cost compared with conventional RAFT agent. Moreover, another important advantage is that the DS is an FDA approved anti-alcoholic drug (ANDA # 086889), which has been widely used in clinical applications for more than 60 years, and recently also been explored and reported as an effective anti-cancer drug.[34–38] We believe that DS, a commercially available, low cost, biocompatible, and FDA approved chemical, is very appealing for the preparation of well-defined biomaterials *via in situ* RAFT polymerization.

In this paper, we report a new generation of *in situ* formed injectable hydrogel system fabricated by a series of newly designed hyperbranched PEG macromers (HP-PEGs) in combination with thiolated hyaluronic acid (HA-SH). The HP-PEGs with numerous pendent acrylate groups were synthesized by an *in situ* RAFT polymerization of PEGDA using Disulfiram (DS) as a RAFT agent precursor. HA-SH was used to crosslink with the HP-PEGs to generate injectable hydrogels *via* thiol-ene click reaction. The gelation time, mechanical properties, swelling and degradation

profile, and antifouling property were studied in detail. Furthermore, the behaviours of adipose-derived stem cells (ADSCs) encapsulated in the hydrogel were evaluated. The efficacy of the HP-PEG/HA-SH/ADSC system for the treatment of diabetic wound healing was assessed on a humanized excisional diabetic wound model in rats.

2. Materials and Methods

2.1 Differentiation test for ADSCs encapsulated in the HP-PEG$_1$/HA-SH hydrogel

Immunofluorescence for Oct4, Sox2, and Nanog for ADSCs was carried out to detect the undifferentiated status. HP-PEG/HA-SH/ADSCs was first fixed with 4% paraformaldehyde, and then reacted with antibodies against Oct4, Sox2, and Nanog. After washed with PBS/Triton X-100, the hydrogel reacted with corresponding secondary antibodies, and counterstained with DAPI. Immunofluorescence was observed with a fluorescence microscope.

For *in vitro* differentiation assessment, ADSCs were induced by relative induction media and media without growth factors, separately.

Adipogenic induction medium: Preadipocyte basal medium-2 supplemented with 16.6% FBS, 50 μg mL^{-1} ascorbate-2 phosphate, 10^{-7} M dexamethasone, 50 μM indomethacin, 0.45 mM 3-isobutyl-1-methyl-xanthine and 10 μg mL^{-1} insulin.

Chondrogenic induction medium: add ITS + (Gibco-BRL) and 10 ng mL^{-1} TGF-1 (Preprotech, Rocky Hill, NJ) into MSC differentiation medium - chondrogenic (PT3925).

Osteogenic induction medium: MSC differentiation medium-osteogenic (PT3924) supplemented with 16.6% FBS, 50 μg mL^{-1} ascorbate-2 phosphate), 10^{-8} M dexamethasone and 10 mM -glycerophosphate.

After separate induction, ADSCs were stained by oil red O, Alizarin red, and safranin-O to detect the morphology.

2.2 Growth factors secretion of ADSCs encapsulated in the HP-PEG$_1$/HA-SH hydrogel

Conditioned media was collected from ADSCs seeded in the hydrogels or plated in wells after 1, 4, and 7 days incubation. Angiogenic protein levels of PIGF, VEGF, and TGF-β were quantified using multi-plex ELISA system (Sigma).

2.3 Animals

6-8-week old male Sprague Dawley (SD) rats with body weights range between 180-240 g were

used for subcutaneous hydrogel implantation, and inducing diabetic rat model. Rats were fed ad libitum water and rodent diet, and housed in the Animal Experimentation of the Chinese Academy of Medical Sciences and Peking Union Medical College Institute of Biomedical Engineering-approved animal care guidelines. All procedures were approved by the Chinese Academy of Medical Sciences and Peking Union Medical College Institute of Biomedical Engineering.

2.4 *In vivo* biosafety and degradation profile of HP-PEGs/HA-SH hydrogels in a subcutaneous implantation model

A subcutaneous implantation was used to test the in vivo biosafety and biodegradation of the injectable HP-PEG1/HA-SH (5% w/v) and HP-PEG2/HA-SH hydrogel (5% w/v). After anesthesia with an intraperitoneal injection of 8% chloral hydrate, four incisions with 1 cm full-thickness transverse each were made on both sides of the shaved dorsum of SD rats. Prepared hydrogels (100 μL) were implanted subcutaneously and incisions were closed with 5-0 nylon suture (Ethicon, Somerville, NJ) and covered with a sterile occlusive dressing (Tegaderm; 3M, St. Paul, MN). Wounds were examined every other day and hydrogels were harvested at 3, 7, 11, 14, and 21 days post-wounding. Residual hydrogel was taken and weighted (4 samples for each condition).

2.5 Diabetic animal model

In order to generate diabetic animals, STZ was used to chemically induce healthy SD rats to develop type 1 diabetes *via* cauda vein injection (45 mg kg^{-1} of STZ dissolved in a 0.1 M sodium citrate buffer). Diabetes was verified by serum glucose levels after the injection. Serum glucose level > 16.7 mmol L^{-1} for at least 4 weeks was defined as successfully developed diabetic rat model. The serum glucose levels were tested pre- and post-injection, and every 7 days during the experiments with a blood glucose meter (OneTouch Ultra® Blood Glucose Monitoring System).

2.6 Humanized diabetic wound model and treatment groups

To better mimic the human wound healing process, a splinted excisional wound model was utilized to prevent wound contraction and allow wound healing through re-epithelialization and granulation tissue formation. Briefly, after full thickness excisional skin wound of 1.1 cm diameter circle was created on the dorsum, wound was circumscribed by silicone rings sutured onto the skin surface surrounding the excision area with 5-0 nylon. Four wounds were generated on each animal. Animals were randomized into the following five treatment groups: directly local injection of ADSCs, S&N (INTRASITE◊GEL, a commercially available product from Smith & Nephew), injectable HP-PEG/HA-SH hydrogel, injectable HP-PEG/HA-SH/ADSCs hydrogel, and blank (no treatment) group (n = 16 wounds per treatment group). For the direct ADSCs local injection group, 200 μL (2.5×10^6 cell mL^{-1}) cell suspension was injected subcutaneously around the wound edge. For the injectable hydrogel with (concentration of ADSCs in the hydrogel: 2.5×10^6 cell mL^{-1}) or without ADSCs groups, 200 μL solution was injected directly onto the wound surface.

Digital images were taken at scheduled time points (days 0, 11, 21 post-procedure). The wound area was measured by two blinded evaluators *via* Image J software (n = 8 wounds for each condition). Wound closure rate (%) was defined as: (origin wound area - residual wound area at day 'X') / origin wound area × 100%.

2.7 Histological analysis

At scheduled time points, wound tissues were excised and immediately fixed in 4% formaldehyde/PBS solution overnight. Samples were then dehydrated with a graded series of ethanol and embedded in paraffin. Tissues were then sectioned into slices with a thickness of 5 μm and stained by hematoxylin and eosin (H&E, Sigma-Aldrich), and Masson's trichrome (Sigma-Aldrich) and visualized by an optical microscope.

Masson's trichrome stained sections were utilized to measure the newly formed dermis thickness, using the Image J software (n = 8 wounds for each condition) with a minimum of 6 measurements per sample. Percentage of neo-dermis thickness (%) was calculated as (neo-dermis thickness / the surrounded normal dermis thickness) × 100%.

2.8 Immunohistochemistry and immunofluorescence

For the immunohistochemical staining, 5 μm thickness paraffin sections were deparaffinized, washed three times in PBS for 5 min. Then the sections were blocked with 5% serum for 30 min. Next, the slides were incubated in primary antibodies, anti-Keratin 10 (1:300), CD31 (1:200), α-SMA (1:25), VEGF (1:50), CD11b (1:100), TNF-α (1:200), and IL-1β (1:200). All tissues were imaged at 400 ×, five high power microscopic fields for each separate wound sample by three blinded evaluators. The inflammation response was identified by the expression of inflammatory cytokines which was quantified by the positively stained cells. Vascularization was evaluated by counting CD31-positive and α-SMA positive staining cells. Re-epithelialization rate was defined as: (the length of newly formed epidermis of both sides /original wound length) × 100%.

Immunofluorescence was also performed after sections' fixation in aceton at -20 ºC. TNF-α, CD31, and α-SMA antibodies were used to perform the immunofluorescent staining. Nuclei were stained with DAPI (purchased from Abcam Inc.). Immunofluorescence images were acquired with an AxioCam HRm camera mounted on a Zeiss Imager M2 microscope.

2.9 Statistical analysis

All values are expressed as mean ± standard deviation (SD). Statistical differences between two groups were determined using the student's unpaired *t* test. A p value < 0.05 was considered statistically significant.

3. Results and discussion

3.1 Multifunctional HP-PEG polymer synthesis

In order to explore the optimal reaction condition of *in situ* RAFT polymerization, six batches of polymerizations were carried out as shown in Supplementary table 1. Firstly, two reactions as controls were carried out without the use of 2,2'-Azobis(2-methylpropionitrile) (AIBN) (Entry 1) or DS (Entry 2), respectively. Entry 1 showed no sign for the occurrence of polymerization as no polymer peak was detected by GPC even after 24 h, while Entry 2 formed a crosslinked network rapidly within 15 min indicating an uncontrollable reaction behaviour. Then, two ratios (1:2 and 1:1.4) of DS to AIBN as well as different reaction temperatures were evaluated for the *in situ* RAFT polymerization of PEGDA (Entry 3-6). As shown in Figure 2A-2D, the polymer mixtures are still soluble even when the monomer conversion was up to 60% for all the four systems, demonstrating the critical roles of DS in the reaction to *in situ* form the RAFT agents. Such high monomer conversion is unexpected given the Flory-Stockmayer theory predicted that such system will be gelled at low monomer conversion. Similar results were also reported in our previous work [6,19,21–23] and attributed to the kinetic control over the chain growth, inter-/intra- molecular crosslinking. Moreover, polymerization process shows a two-stage growth behaviour. At the early stage (monomer conversion less than 40%), Mw increased with monomer conversion in a linear manner and the GPC traces (Figure S1) showed single peaks with a low PDI. While in the later stage, the Mw increased rapidly and GPC peaks showed a multiple peaks with a high PDI, indicating the occurrence of the intermolecular crosslinking, combination of the polymer chains in the reaction system. [22,23]

The reaction kinetic was studied by varying the AIBN/DS ratio and temperature. As shown in Figure 2E, more AIBN feeding results in a much faster polymerization rate and a higher PDI at the same conversion. Thus, the feeding ratio of 1:1.4 (molar ratio of DS: I) was selected to delay the later stage of polymerization compared with the feeding ratio of 1:2. Similarly, the optimized reaction temperature is selected at 70 ^{o}C.

The samples taken from Entry 4 were purified, and the polymer structure was characterized in detail. HP-PEGs with molecular weights of 10 and 20 kDa (termed as HP-PEG$_1$ and HP-PEG$_2$, respectively) were obtained. From the GPC results, the value of Mark-Houwink exponent (α) is 0.29 for HP-PEG$_1$ and 0.30 for HP-PEG$_2$, respectively (Figure S2), lower than characteristic α of a linear structure (more than 0.5), indicating a sphere-shaped morphology, suggesting the formation of branched structure. ^{1}H-NMR results show the existence of the acrylate moieties in the purified HP-PEG$_1$ and HP-PEG$_2$ (Figure 2 and Figure S4). Based on the comparison of the amount of pendent unit with the amount of entire monomer repeating units, the branch ratios were calculated, which showed values of approximately 32% and 45% (Figure S3), respectively. We can also observe from the ^{1}H-NMR spectrum of a purified HP-PEG$_1$ polymer that the peaks of DS and AIBN moieties can be found within the polymer chains, which reveals that the polymerization follows the proposed *in situ* RAFT polymerization (Figure 2F).

3.2 Injectable HP-PEG/HA-SH hydrogels

PEG/HA hydrogels have been studied in the field of tissue engineering for years. Shea *et al.* designed a PEG/HA hydrogel by photopolymerization and used as a non-viral

gene delivery vector;[39] Webb *et al.* developed a semi-interpenetrating PEG/HA hydrogel to support 3D cell culture for cell therapy applications.[40] These PEG macromers are suffered from low functional group density, resulting in a compromised crosslinking degree; besides, the crosslinker synthetic pathways are complicated. Thus, we utilized our HP-PEGs to crosslink with HA-SH to fabricate *in situ* formed hydrogels *via* Michael addition reaction. HA-SH is a widely used derivative of HA, which possesses the biological and regenerative properties of HA, and also can crosslink with acrylate groups spontaneously *via* Michael addition under physiological conditions. As expected, rapid gelation occurs when the acrylate groups from the polymer reacting with the thiol groups from the HA-SH. The hydrogels are transparent and easy to be handled. Gelation time of both HP-PEG/HA-SH hydrogels was examined using the stirring method. Both hydrogels exhibit fast gelation time at various concentrations (2.5%, 5%, and 10% w/v) and the higher concentration showed faster gelation rate (Figure 3A). For example, the gelation time is about 96 seconds for 2.5% (w/v) HP-PEG$_1$ polymer versus 57 seconds for 10% (w/v) polymer HP-PEG$_1$. The rapid gelation demonstrated the suitability as injectable hydrogels, which has potential to address current needs for clinical use of biomaterials.[41,42] By adjusting the pendent acrylate content and polymer concentration, the gelation time can be adjusted to meet the needs of a specific tissue engineering application.

To reveal the mechanical properties of HP-PEG/HA-SH hydrogels, rheological measurements were performed during the gelation process sequentially using time and frequency sweep (Figure 3B and Figure S5). Typically, at the concentration of 5%,

HP-PEG_1/HA-SH exhibit approximate 136 Pa of storage modulus which is within the range of storage modulus of soft tissue (Figure 3C). Both hydrogels showed low frequency dependence (Figure S6 and Figure S7) for all concentrations, demonstrating that the hydrogels are highly elastic.[7] Proper mechanical properties can support the encapsulated cells with a favorable environment as well as no extra burden to the host tissues.

To study the hydrogel swelling and degradation properties *in vitro*, the hydrogel samples (5% (w/v)) were incubated in PBS buffer at 37 ^{o}C. After the hydrogels reached their equilibrium swelling levels within 1 day, their wet weight remained almost constant for 4 days. The hydrogels then showed slight swelling within 40 days (1.9-time of original weight) (Figure 3D). The hydrogels underwent remarkable swelling and became shapeless after 40 days. The hydrogel structure started to break and finally disappeared after it reached the maximum water retention ability. Thus, we successfully obtained a non-swelling hydrogel system, which avoids the limitations of weak mechanical toughness caused by swelling. This kind of non-swelling profile, in a relatively long time period, will result in less medical complications caused by high hydrogel swelling ratios, which is a desirable advantage of hydrogels being applied onto wound sites.

To investigate the porosity and morphology of the hydrogel, SEM were used to capture the microstructure. The HP-PEG/HA-SH hydrogels show a microporous sponge-like structure with the pore size ranging from 5 to 20 μm (Figure S8).

We also tested the antifouling property of our hydrogel systems, because the PEG

derivatives have been proved to be an antifouling biomedical material due to its biocompatibility and hydrophilicity. The HP-PEG_1/HA-SH hydrogel exhibits a relatively lower amount of protein adsorption than the collagen/chitosan hydrogel and HP-PEG_1 hydrogel (formed by UV curing) from 2 to 24 h incubation period with FBS solution (Figure 3E). The well-maintained antifouling property endows the hydrogel with the ability to mitigate the effects of the foreign body response after implantation. In view of the suitable mechanical stability, the injectable profile, and the non-swelling and antifouling properties, we believe this hydrogel system to have chemical advantages and potential satisfaction for both medical specialists and patients, providing it with great superiority as an alternative biomaterial for wound healing.

3.3 Biocompatibility of HP-PEG/HA-SH hydrogels

To determine the biocompatibility of HP-PEG polymers and HP-PEG/HA-SH hydrogels, 3T3 and ADSCs were used for *in vitro* cell viability tests by alamarBlue assay. Both cell lines showed high cell viability when cocultured with different polymer concentrations (Figure S9). The cytotoxicity test for the hydrogels were conducted by seeding the cells into the HP-PEG/HA-SH hydrogels and evaluated by alamarBlue assay. Both hydrogels exhibited high cell viability for both cell lines (Figure S10), indicating that this *in situ* hydrogel system did not show toxicity on the cells. We also performed *in vivo* biosafety and degradation test of both hydrogels. After implantation, no signs of infection, inflammation or rejection were detected. The hydrogels exhibited minimal swelling and a slow degradation rate within 21 days (Figure S11). In the current study, we selected HP-PEG_1/HA-SH hydrogel with 5%

(w/v) exhibiting 68 seconds of gelation time, and 125 Pa storage modulus for the following *in vitro* and *in vivo* investigations.

3.4 ADSCs' behaviors in HP-PEG/HA-SH hydrogels

Stem cell therapy has been proven to be safe and efficient by many researchers and preclinical studies due to their unique features, such as self-renewal and differentiation potential.[3,43,44] Among various types of stem cells, ADSCs are of great interest as they can be easily isolated from the abundant source of fat tissue, and possess characteristics resembling those of mesenchymal stem cells. Besides, ADSCs have the potential to promote tissue regeneration through secreting essential factors to stimulate angiogenesis and re-epithelialization.[3,45] However, the maintenance of cell viability and stemness is an urgent issue to be solved under the hostile environment of DFUs. We then further detected the ADSCs' behaviors (self-renewal and secretion ability) in this hydrogel system. The expression of Oct4, Sox2, and Nanog, which are key regulators for maintenance of self-renewal and multipotency of ADSCs,[7,46] was verified by immunological staining method (Figure 4A). Most of the ADSCs are showing positively stained Oct4, Sox2, or Nanog after 2, 5, and 7 days seeding in the hydrogel. We also assessed the differentiation status of the encapsulated ADSCs with or without specific induction media. After induction, ADSCs are directed to differentiate into adipogenic, osteogenic, and chondrogenic lineages, verified by the staining of oil red O, safranin-O, and alizarin red staining, respectively (Figure 4B), while the ADSCs, without induction, showed no sign of differentiation. These data demonstrated that ADSCs maintained their stemness well even in the hydrogel. The protein level of

pro-angiogenic growth factors was detected on conditioned media from hydrogel and plated culture conditions. It can be noted that the protein levels of PIGF, VEGF, and TGF-β were increased from day 1 to day 7 in both conditioned media (Figure 4C, D, and E). PIGF expression was found to be significantly increased at day 7 in hydrogel cultured ADSCs compared to those cultured in standard conditions. VEGF and TGF-β expression was found to significantly increased at day 1 and day 4. The ability of maintaining the multi-potency and secretion capacity of wound healing associated growth factors of these encapsulated ADSCs in the HP-PEG-based hydrogel exhibits potential therapeutic value in regenerative medicine, indicating the possibility of the combination therapy in promoting wound healing.

3.5 HP-PEG/HA-SH/ADSCs promotes humanized diabetic wound healing process

To test the efficiency of the injectable HP-PEG/HA-SH hydrogel in promoting wound healing, a humanized excisional wound model, which can better mimic human skin wound repair mechanisms[47], was developed in the Streptozotocin induced diabetic SD rats. To validate our hypothesis that the HP-PEG/HA-SH/ADSCs system can accelerate diabetic wound healing, no-treatment (blank), and treatment with INTRASITE$^{◊}$GEL (a commercially available product from Smith & Nephew (S&N)), direct local injection of ADSCs, and injectable HP-PEG/HA-SH hydrogel (blank hydrogel) were used as controls to bolster the comparison. The treatment process by injectable hydrogel was recorded as Supplementary movie 1. Wound closure rate (%) was defined as: (origin wound area - residual wound area at day ‘X’) / origin wound area × 100%. In the present study, the wounds treated with HP-PEG/HA-SH/ADSCs

showed significantly accelerated wound closure rate than no treatment wounds (1.9- and 1.4-fold faster) and cell only treated wounds (1.3- and 1.3-fold faster) at days 11 and 21 post-wounding (Figure 5A and B). H&E staining sections show that, HP-PEG/HA-SH/ADSCs treated wounds yielded an accelerated healing rate compared with the no treatment wounds, as proved by the formation of a thicker granular tissue (Figure 5C). We then performed Masson's trichrome assay (Figure 5D) to further understand the dermis deposition which provides the initial support for cell migration. HP-PEG/HA-SH/ADSCs hydrogel treated wounds regenerated a much thicker dermis than no treatment wounds (95.2% ± 1.7 vs 42.2% ± 3.4, $p<0.01$) and cell only treated wounds (95.2% ± 1.7 vs 75.5% ± 7.3, $p<0.01$) (Figure 5E). Additionally, collagen remodeling in the ADSCs alone and HP-PEG/HA-SH/ADSCs hydrogel treated wounds is more homogenous than other groups.

The prolonged inflammation, reduced vascular formation, and non-migratory epidermis in diabetic wound beds are considered to be essential factors in impaired and delayed diabetic wound healing. To further study the mechanism behind the accelerated healing, we performed immunohistochemistry or immunofluorescence assays for the wound tissues. Inflammatory factors (CD11b, TNF α, IL-1β) expression were significantly inhibited at days 11 and 21 in HP-PEG/HA-SH/ADSCs hydrogel treated wounds, indicating the prolonged inflammatory phase is reversed (Figure 6A, Figure S12 and Figure 7). To study the angiogenesis behaviours during the healing, protein expression of key factors related to vascular development (VEGF, CD31, and α-SMA) were detected. The number of CD31 and α-SMA positive stained vessels of each wound

was counted (Figure 6B and Figure 6C), respectively. $CD31^+$ and α-SMA^+ vessel densities were significantly higher in HP-PEG/HA-SH/ADSCs hydrogel treated wounds at day 21. VEGF expression also indicated a higher level in HP-PEG/HA-SH/ADSCs hydrogel treated wounds demonstrating a positive effect for angiogenesis (Figure 6D). Enhanced re-epithelialization rate was evidenced by the gap-junctional connections of keratinocytes layers (Figure 6E and Figure S13) at day 21. There are also significant differences between cell only and hydrogel/cell treated wounds, such as increased neodermis thickness, inhibited inflammatory factors expression, enhanced CD31 and VEGF expression and re-epithelialization at 21 days from Figure 6. Based on the histological assays, the HP-PEG/HA-SH/ADSCs system presented significant advantages for diabetic wound healing, including prevention of persistent inflammation, promotion of vasculogenesis, and re-epithelialization compared to the wounds without treatment.

4. Conclusion

In this report, we have described the development of an new injectable hydrogel platform as a stem cell delivery and retention system. The *in situ* RAFT polymerization of PEGDA using DS as a RAFT agent precursor endows the resultant hyperbranched PEG polymers good biocompatibility and abundant pendent acrylate groups, which can be utilized to form an injectable hydrogel with a rapid gelation rate and a tunable mechanical property. The HP-PEG/HA-SH hydrogels also demonstrated non-swelling and antifouling properties, as well as well-retained stem cell properties *in vitro*. Furthermore, this versatile hydrogel system encapsulated with ADSCs

exhibited an accelerated diabetic wound healing process through inhibiting inflammation, promoting angiogenesis and re-epithelialization.

Acknowledgements

Q.X. and S.A. contributed equally to this manuscript. We gratefully acknowledge Professor Laifeng Song (Cardiovascular Institute and Fuwai Hospital, Chinese Academy of Medical Sciences and Peking Union Medical College, China) for the kind guidance of tissue morphology and histology analysis. We also acknowledge the technical support of Dr. Ian Reid and Mr. Matteo Nicolasi from the Nano Imaging and Material Analysis Centre, University College Dublin. This work was supported by Science Foundation Ireland (No 13/IA/1962, 10/IN.1/B2981(T), 15/IFA/3037), Health Research Board of Ireland (HRA-POR-2013-412), University College Dublin and DEBRA Ireland, National Natural Science Foundation of China (No. 51573129 and No. 51473117), and National Natural Science Funds for Distinguished Young Scholar (No. 51325305).

References

[1] A.J. Boulton, L. Vileikyte, G. Ragnarson-Tennvall, J. Apelqvist, The global burden of diabetic foot disease, Lancet. 366 (2005) 1719–1724. doi:10.1016/S0140-6736(05)67698-2.

[2] V. Falanga, Wound healing and its impairment in the diabetic foot, Lancet. 366 (2005) 1736–1743. doi:10.1016/S0140-6736(05)67700-8.

[3] W.U. Hassan, U. Greiser, W. Wang, Role of adipose-derived stem cells in wound healing, Wound Repair Regen. 22 (2014) 313–325.

doi:10.1111/wrr.12173.

[4] J.A. Burdick, R.L. Mauck, S. Gerecht, To Serve and Protect: Hydrogels to Improve Stem Cell-Based Therapies, Cell Stem Cell. 18 (2016) 13–15. doi:10.1016/j.stem.2015.12.004.

[5] S. Zhu, J. Wang, H. Yan, Y. Wang, Y. Zhao, B. Feng, K. Duan, J. Weng, An injectable supramolecular self-healing bio-hydrogel with high stretching, extensibility, ductility and swelling ratio, J. Mater. Chem. B. 5 (2017) 6977–7206. doi:10.1039/C7TB01183K.

[6] Y. Dong, Y. Qin, M. Dubaa, J. Killion, Y. Gao, T. Zhao, D. Zhou, D. Duscher, L. Geever, G.C. Gurtner, W. Wang, A rapid crosslinking injectable hydrogel for stem cell delivery, from multifunctional hyperbranched polymers via RAFT homopolymerization of PEGDA, Polym. Chem. 6 (2015) 6182–6192. doi:10.1039/C5PY00678C.

[7] Y. Dong, A. Sigen, M. Rodrigues, X. Li, S.H. Kwon, N. Kosaric, S. Khong, Y. Gao, W. Wang, G.C. Gurtner, Injectable and Tunable Gelatin Hydrogels Enhance Stem Cell Retention and Improve Cutaneous Wound Healing, Adv. Funct. Mater. 27 (2017) 1–12. doi:10.1002/adfm.201606619.

[8] F.P. Brandl, A.K. Seitz, J.K. V Teßmar, T. Blunk, A.M. Göpferich, Enzymatically degradable poly(ethylene glycol) based hydrogels for adipose tissue engineering, Biomaterials. 31 (2010) 3957–3966. doi:10.1016/j.biomaterials.2010.01.128.

[9] C. Hiemstra, L.J. Van Der Aa, Z. Zhong, P.J. Dijkstra, J. Feijen, Rapidly in

situ-forming degradable hydrogels from dextran thiols through Michael addition., Biomacromolecules. 8 (2007) 1548–1556. doi:10.1021/bm061191m.

[10] Y. Zheng, S. Li, Z. Weng, C. Gao, Hyperbranched polymers: advances from synthesis to applications, Chem. Soc. Rev. 44 (2015) 4091–4130. doi:10.1039/C4CS00528G.

[11] J. Yang, J. Yeom, B. Woo, A.S. Hoffman, S. Kwang, In situ -forming injectable hydrogels for regenerative medicine, Prog. Polym. Sci. 39 (2014) 1973–1986. doi:10.1016/j.progpolymsci.2014.07.006.

[12] J.L. Drury, D.J. Mooney, Hydrogels for tissue engineering: Scaffold design variables and applications, Biomaterials. 24 (2003) 4337–4351. doi:10.1016/S0142-9612(03)00340-5.

[13] L.I.F. Moura, A.M.A. Dias, E. Carvalho, H.C. de Sousa, Recent advances on the development of wound dressings for diabetic foot ulcer treatment—A review, Acta Biomater. 9 (2013) 7093–7114. doi:10.1016/j.actbio.2013.03.033.

[14] N.Q. Tran, Y.K. Joung, E. Lih, K.D. Park, In situ forming and rutin-releasing chitosan hydrogels as injectable dressings for dermal wound healing, Biomacromolecules. 12 (2011) 2872–2880. doi:10.1021/bm200326g.

[15] B. Balakrishnan, M. Mohanty, P.R. Umashankar, A. Jayakrishnan, Evaluation of an in situ forming hydrogel wound dressing based on oxidized alginate and gelatin, Biomaterials. 26 (2005) 6335–6342. doi:10.1016/j.biomaterials.2005.04.012.

[16] A.S. Hoffman, Hydrogels for biomedical applications, Adv. Drug Deliv. Rev. 64

(2012) 18–23. doi:10.1016/j.addr.2012.09.010.

[17] J.A. Hunt, R. Chen, T. van Veen, N. Bryan, Hydrogels for tissue engineering and regenerative medicine, J. Mater. Chem. B. 2 (2014) 5319–5338. doi:10.1039/C4TB00775A.

[18] P.A. Costello, I.K. Martin, A.T. Slark, D.C. Sherrington, A. Titterton, Branched methacrylate copolymers from multifunctional monomers: chemical composition and physical architecture distributions, Polymer (Guildf). 43 (2002) 245–254. doi:10.1016/S0032-3861(01)00581-X.

[19] W. Wang, Y. Zheng, E. Roberts, C.J. Duxbury, L. Ding, D.J. Irvine, S.M. Howdle, Controlling chain growth: A new strategy to hyperbranched materials, Macromolecules. 40 (2007) 7184–7194. doi:10.1021/ma0707133.

[20] Y. Zheng, H. Cao, B. Newland, Y. Dong, A. Pandit, W. Wang, 3D single cyclized polymer chain structure from controlled polymerization of multi-vinyl monomers: Beyond flory-stockmayer theory, J. Am. Chem. Soc. 133 (2011) 13130–13137. doi:10.1021/ja2039425.

[21] T. Zhao, H. Zhang, D. Zhou, Y. Gao, Y. Dong, U. Greiser, H. Tai, W. Wang, Water soluble hyperbranched polymers from controlled radical homopolymerization of PEG diacrylate, RSC Adv. 5 (2015) 33823–33830. doi:10.1039/C5RA01253H.

[22] Y. Gao, D. Zhou, T. Zhao, X. Wei, S. McMahon, J. O'Keeffe Ahern, W. Wang, U. Greiser, B.J. Rodriguez, W. Wang, Intramolecular Cyclization Dominating Homopolymerization of Multivinyl Monomers toward Single-Chain

Cyclized/Knotted Polymeric Nanoparticles, Macromolecules. 48 (2015) 6882–6889. doi:10.1021/acs.macromol.5b01549.

[23] T. Zhao, Y. Zheng, J. Poly, W. Wang, Controlled multi-vinyl monomer homopolymerization through vinyl oligomer combination as a universal approach to hyperbranched architectures., Nat. Commun. 4 (2013) 1873. doi:10.1038/ncomms2887.

[24] Y. Gao, B. Newland, D. Zhou, K. Matyjaszewski, W. Wang, Controlled polymerization of multivinyl monomers: toward single chain cyclized/knotted polymer architecture, Angew. Chemie. 56 (2016) 450–460. doi:10.1002/ange.201608786.

[25] Y. Dong, P. Gunning, H. Cao, A. Mathew, B. Newland, A.O. Saeed, J.P. Magnusson, C. Alexander, H. Tai, A. Pandit, W. Wang, Dual stimuli responsive PEG based hyperbranched polymers, Polym. Chem. 1 (2010) 827. doi:10.1039/c0py00101e.

[26] Y. Dong, A.O. Saeed, W. Hassan, C. Keigher, Y. Zheng, H. Tai, A. Pandit, W. Wang, “one-step” preparation of thiol-ene clickable PEG-based thermoresponsive hyperbranched copolymer for in situ crosslinking hybrid hydrogel, Macromol. Rapid Commun. 33 (2012) 120–126. doi:10.1002/marc.201100534.

[27] Y. Dong, W. Hassan, Y. Zheng, A.O. Saeed, H. Cao, H. Tai, A. Pandit, W. Wang, Thermoresponsive hyperbranched copolymer with multi acrylate functionality for in situ cross-linkable hyaluronic acid composite semi-IPN hydrogel, in: J.

Mater. Sci. Mater. Med., 2012: pp. 25–35. doi:10.1007/s10856-011-4496-z.

[28] Y. Dong, W.U. Hassan, R. Kennedy, U. Greiser, A. Pandit, Y. Garcia, W. Wang, Performance of an in situ formed bioactive hydrogel dressing from a PEG-based hyperbranched multifunctional copolymer, Acta Biomater. 10 (2014) 2076–2085. doi:10.1016/j.actbio.2013.12.045.

[29] S. McMahon, R. Kennedy, P. Duffy, J.M. Vasquez, J.G. Wall, H. Tai, W. Wang, Poly(ethylene glycol)-Based Hyperbranched Polymer from RAFT and Its Application as a Silver-Sulfadiazine-Loaded Antibacterial Hydrogel in Wound Care, ACS Appl. Mater. Interfaces. 8 (2016) 26648–26656. doi:10.1021/acsami.6b11371.

[30] J. Chiefari, Y.K.B. Chong, F. Ercole, J. Krstina, J. Jeffery, T.P.T. Le, R.T. a Mayadunne, G.F. Meijs, C.L. Moad, G. Moad, E. Rizzardo, S.H. Thang, Living Free-Radical Polymerization by Reversible Addition−Fragmentation Chain Transfer: The RAFT Process, Macromolecules. 31 (1998) 5559–5562. doi:10.1021/ma9804951.

[31] D.J. Keddie, G. Moad, E. Rizzardo, S.H. Thang, RAFT agent design and synthesis, Macromolecules. 45 (2012) 5321–5342. doi:10.1021/ma300410v.

[32] H. Tai, A. Tochwin, W. Wang, Thermoresponsive hyperbranched polymers via in Situ RAFT copolymerization of peg-based monomethacrylate and dimethacrylate monomers, J. Polym. Sci. Part A Polym. Chem. 51 (2013) 3751–3761. doi:10.1002/pola.26779.

[33] D. Zhou, Y. Gao, A. Sigen, Q. Xu, Z. Meng, U. Greiser, W. Wang, Anticancer

Drug Disulfiram for in Situ RAFT Polymerization: Controlled Polymerization, Multifacet Self-Assembly, and Efficient Drug Delivery, ACS Macro Lett. 5 (2016) 1266–1272. doi:10.1021/acsmacrolett.6b00777.

[34] R.C. de Melo, R. Lopes, J.C. Alves, A case of psychosis in disulfiram treatment for alcoholism., Case Rep. Psychiatry. 2014 (2014) 561092. doi:10.1155/2014/561092.

[35] B. Sezgin, S. Sibar, H. Bulam, K. Findikcioglu, S. Tuncer, B. Dogan, Disulfiram Implantation for the Treatment of Alcoholism: Clinical Experiences from the Plastic Surgeon's Point of View, Arch. Plast. Surg. 41 (2014) 571–575. doi:10.5999/aps.2014.41.5.571.

[36] R.K. Fuller, H.P. Roth, Disulfiram for the treatment of alcoholism. An evaluation in 128 men, Ann. Intern. Med. 90 (1979) 901–904. doi:10.7326/0003-4819-90-6-901.

[37] M. Goldstein, B. Anagnoste, E. Lauber, M.R. McKereghan, Inhibition of dopamine- β -hydroxylase by disulfiram, Life Sci. 3 (1964) 763–767. doi:10.1016/0024-3205(64)90031-1.

[38] Z. Skrott, M. Mistrik, K.K. Andersen, S. Friis, D. Majera, J. Gursky, T. Ozdian, J. Bartkova, Z. Turi, P. Moudry, M. Kraus, M. Michalova, J. Vaclavkova, P. Dzubak, I. Vrobel, P. Pouckova, J. Sedlacek, A. Miklovicova, A. Kutt, J. Li, J. Mattova, C. Driessen, Q.P. Dou, J. Olsen, M. Hajduch, B. Cvek, R.J. Deshaies, J. Bartek, Alcohol-abuse drug disulfiram targets cancer via p97 segregase adaptor NPL4, Nature. 552 (2017) 194–199. doi:10.1038/nature25016.

[39] J.A. Wieland, T.L. Houchin-Ray, L.D. Shea, Non-viral vector delivery from PEG-hyaluronic acid hydrogels, J. Control. Release. 120 (2007) 233–241. doi:10.1016/j.jconrel.2007.04.015.

[40] H.-J. Lee, A. Sen, S. Bae, J.S. Lee, K. Webb, Poly(ethylene glycol) diacrylate/hyaluronic acid semi-interpenetrating network compositions for 3-D cell spreading and migration, Acta Biomater. 14 (2015) 43–52. doi:10.1016/J.ACTBIO.2014.12.007.

[41] E.J. Chen, J. Novakofski, W. Kenneth Jenkins, W.D. O'Brien, Young's modulus measurements of soft tissues with application to elasticity imaging, IEEE Trans. Ultrason. Ferroelectr. Freq. Control. 43 (1996) 191–194. doi:10.1109/58.484478.

[42] A. Samani, J. Bishop, C. Luginbuhl, D.B. Plewes, Measuring the elastic modulus of ex vivo small tissue samples, Phys. Med. Biol. 48 (2003) 2183–2198. doi:10.1088/0031-9155/48/14/310.

[43] W.-S. Kim, B.-S. Park, J.-H. Sung, J.-M. Yang, S.-B. Park, S.-J. Kwak, J.-S. Park, Wound healing effect of adipose-derived stem cells: a critical role of secretory factors on human dermal fibroblasts., J. Dermatol. Sci. 48 (2007) 15–24. doi:10.1016/j.jdermsci.2007.05.018.

[44] A.M. Altman, Y.S. Yan, N. Matthias, X.W. Bai, C. Rios, A.B. Mathur, Y.-H.H. Song, E.U. Alt, IFATS Collection: Human Adipose-Derived Stem Cells Seeded on a Silk Fibroin-Chitosan Scaffold Enhance Wound Repair in a Murine Soft Tissue Injury Model, Stem Cells. 27 (2009) 250–258.

doi:10.1634/stemcells.2008-0178.

[45] M. Teng, Y. Huang, H. Zhang, Application of stems cells in wound healing - An update, Wound Repair Regen. 22 (2014) 151–160. doi:10.1111/wrr.12152.

[46] K. Gwon, E. Kim, G. Tae, Heparin-hyaluronic acid hydrogel in support of cellular activities of 3D encapsulated adipose derived stem cells, Acta Biomater. 49 (2017) 284–295. doi:10.1016/j.actbio.2016.12.001.

[47] V.W. Wong, M. Sorkin, J.P. Glotzbach, M.T. Longaker, G.C. Gurtner, Surgical Approaches to Create Murine Models of Human Wound Healing, J. Biomed. Biotechnol. 2011 (2011) 1–8. doi:10.1155/2011/969618.

Figures and figure caption

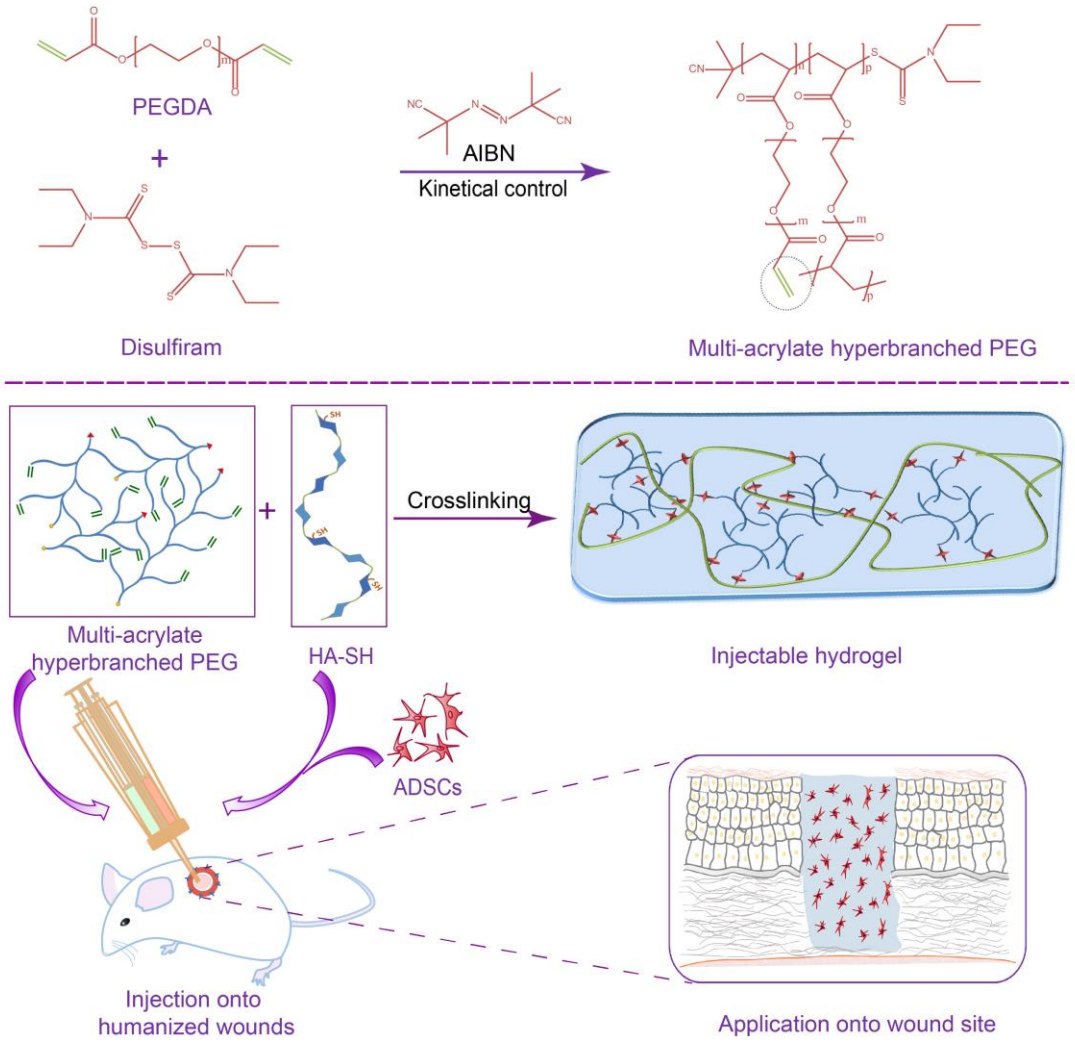

Figure 1. Schematic concepts of the generation and application of injectable HP-PEG-based hydrogel. Scheme illustrates the synthesis of the HP-PEG polymers by *in situ* RAFT polymerization using AIBN as the initiator and DS as the precursor of RAFT agent. The hydrogel is *in situ* formed *via* thiol-ene reaction by mixing HP-PEG with HA-SH. ADSCs are encapsulated in the hydrogel and the hydrogel system is applied onto a humanized diabetic wound model.

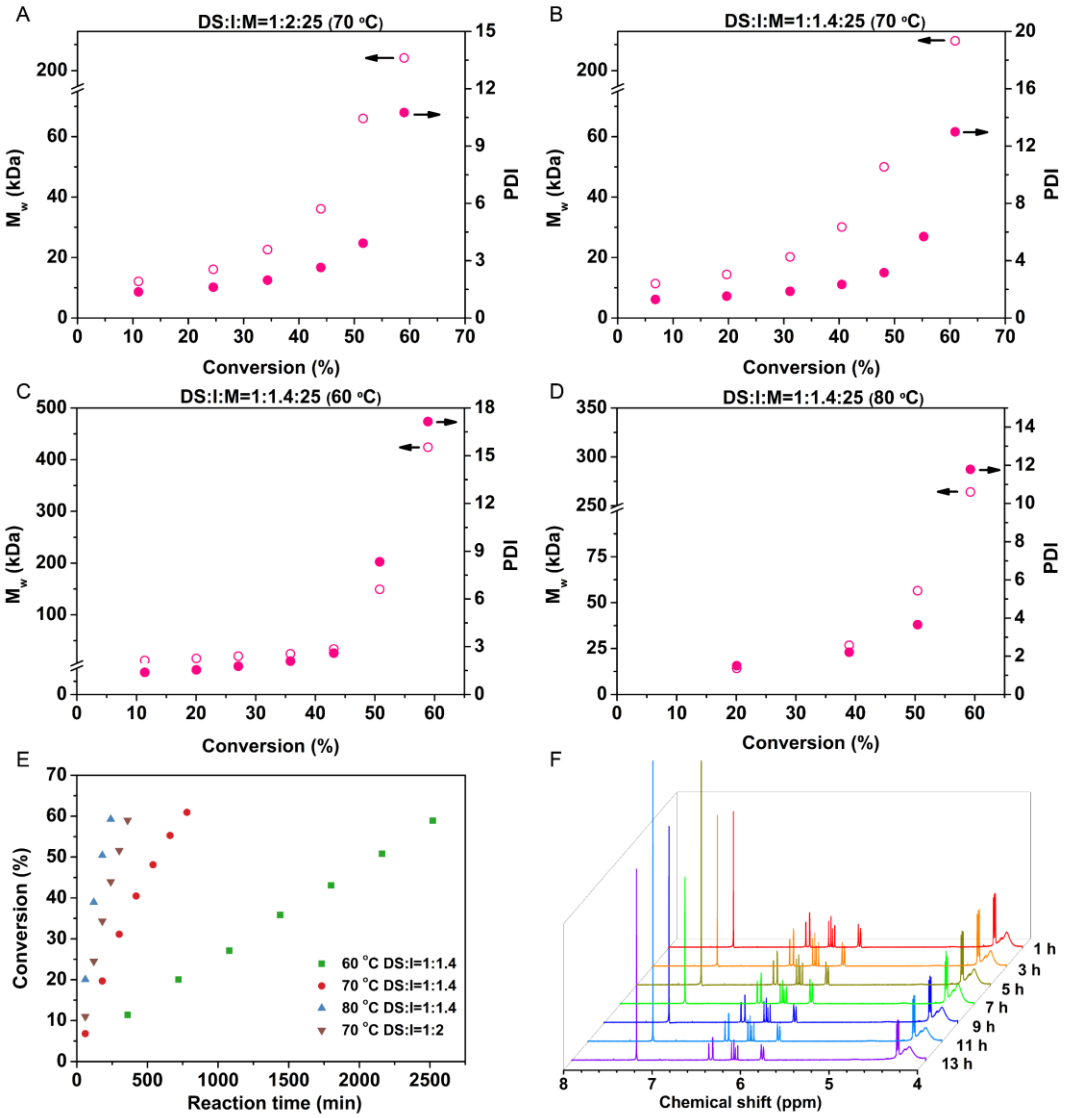

Figure 2. Kinetic plots for *in situ* RAFT polymerization of PEGDA. A-D, Dependence of the molecular weight (Mw) and polydispersity index (PDI) on the monomer conversion for the *in situ* RAFT polymerization. A, entry 3. B, entry 4. C, entry 5. D, entry 6. E, Conversion of HP-PEG versus reaction time. The monomer conversion increasing with reaction time; F, Zoom in areas of ^{1}H-NMR spectrums of purified polymer samples taken from entry 4.

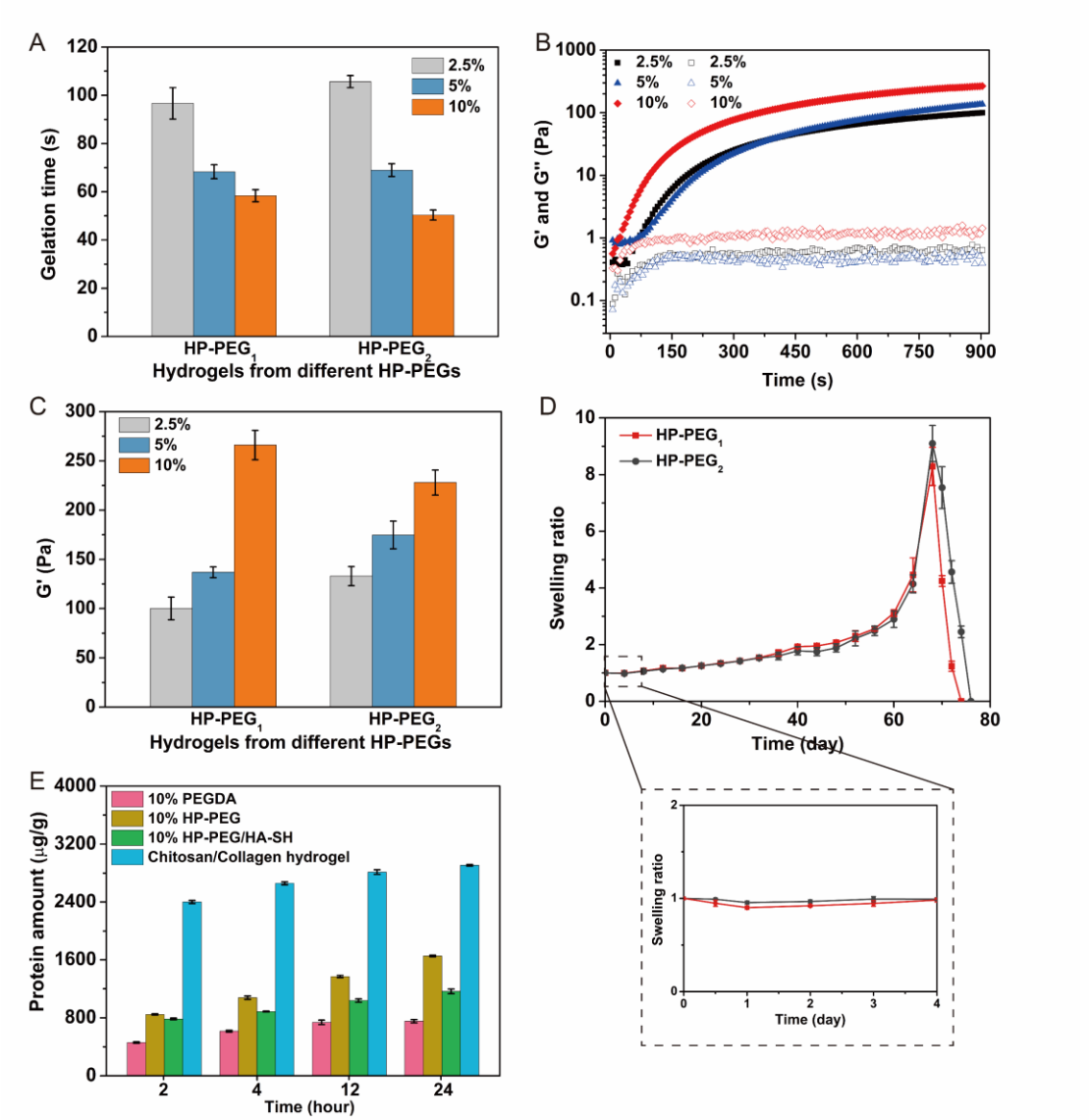

Figure 2. Properties of HP-PEG/HA-SH hydrogels. A, Gelation time of HP-PEG/HA-SH hydrogels. B, Gelation process of HP-PEG$_1$/HA-SH hydrogel characterized by rheometer. C, Storage modulus of injectable HP-PEG/HA-SH hydrogels at different concentrations D, Swelling behaviour of injectable HP-PEG/HA-SH hydrogels obtained by incubating in PBS at 37 ^{o}C. After 60 days, the hydrogels showed shapeless, loose property and finally disappeared at approximately 75 days. E, Evaluation of protein adsorption on hydrogels determined by Micro BCA protein assay.

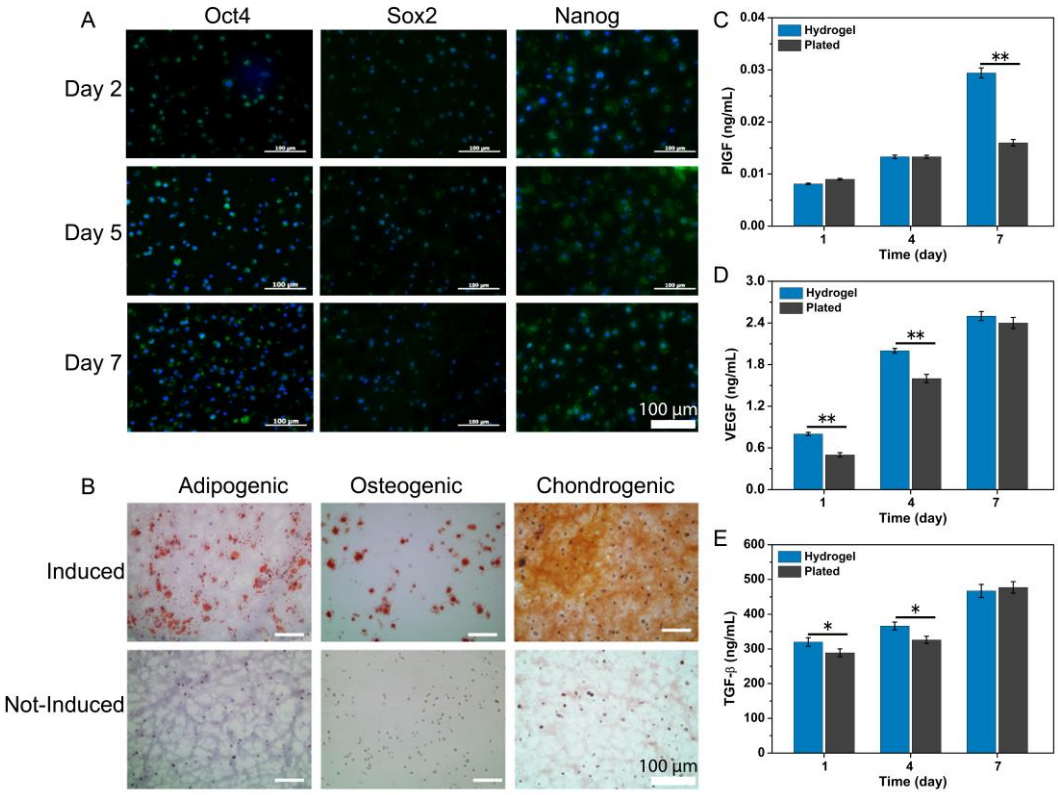

Figure 4. Stemness and secretion of the ADSCs in HP-PEG/HA-SH hydrogel. A, Immunological staining images for Oct4, Sox2, and Nanog of ADSCs encapsulated in the hydrogels after 2, 5, and 7 days post-encapsulation. B, Differentiation status of ADSCs in the hydrogel into adipogenic, osteogenic, and chondrogenic lineages using oil red O, Alizarin red, and safranin-O staining. C, D, and E, Protein levels of PIGF, VEGF, and TNF-β in conditioned media from ADSCs cultured in hydrogels compared to those plated under standard conditions. Scale bar, A and B, 100 μm. *, $p<0.05$; **, $p<0.01$.

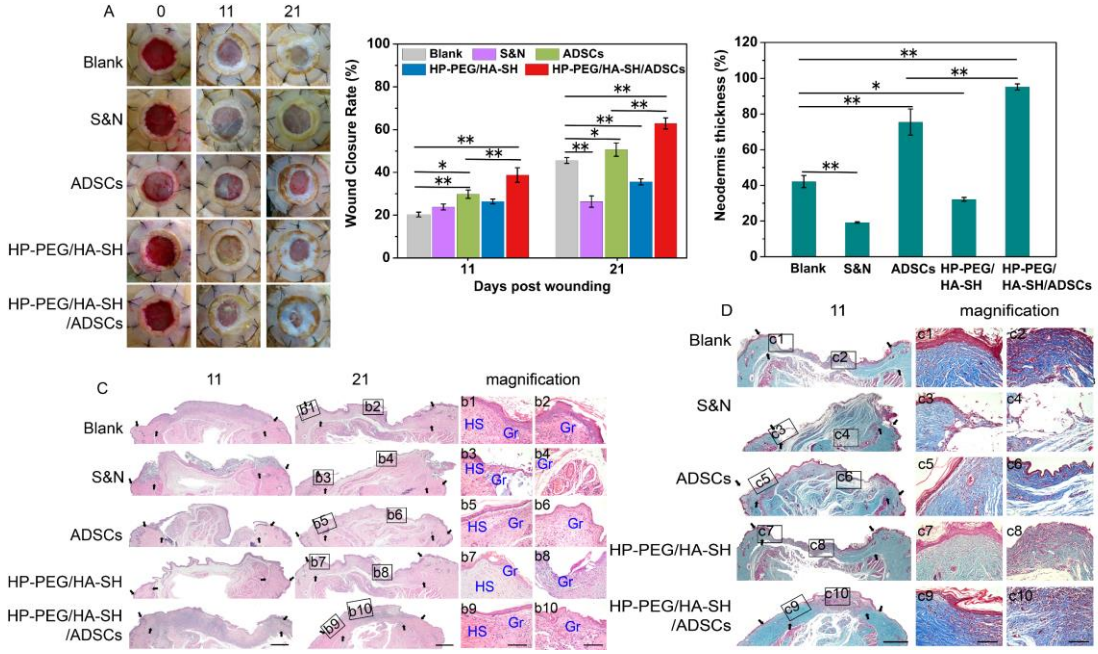

Figure 5. Treatments with humanized excisional wound model in diabetic rats. A, Representative images of wounds during 21-day *in vivo* experiments. B, Quantification of wound closure rate (%) over 21-day period. C, H&E staining of wounds at days 11 and 21 post-wounding. The sites of initial tissue injury are indicated by arrows. Magnifications of the corresponding boxed areas at day 21 are shown in the right, respectively. HS and Gr are represented as healthy skin and granulation matrix. D, Masson's trichrome staining of full-length wound sections at 21 days post-wounding. Magnifications of the corresponding boxed areas are shown in the right, respectively. E, Percentages of newly-formed tissue thickness at 21 days post-wounding. Injectable HP-PEG/HA-SH/ADSCs hydrogel treated wounds show significantly promoted healing than the no-treatment wounds (n = 8 for each condition). Histological sections show a more homogenous morphology of tissues and thicker collagen deposition in the injectable HP-PEG/HA-SH/ADSCs hydrogel treated wounds. Scale bars: C and D, 1 mm; (c1)-(c10) and (d1)-(d10), 100 μm. *, $p<0.05$; **, $p<0.01$.

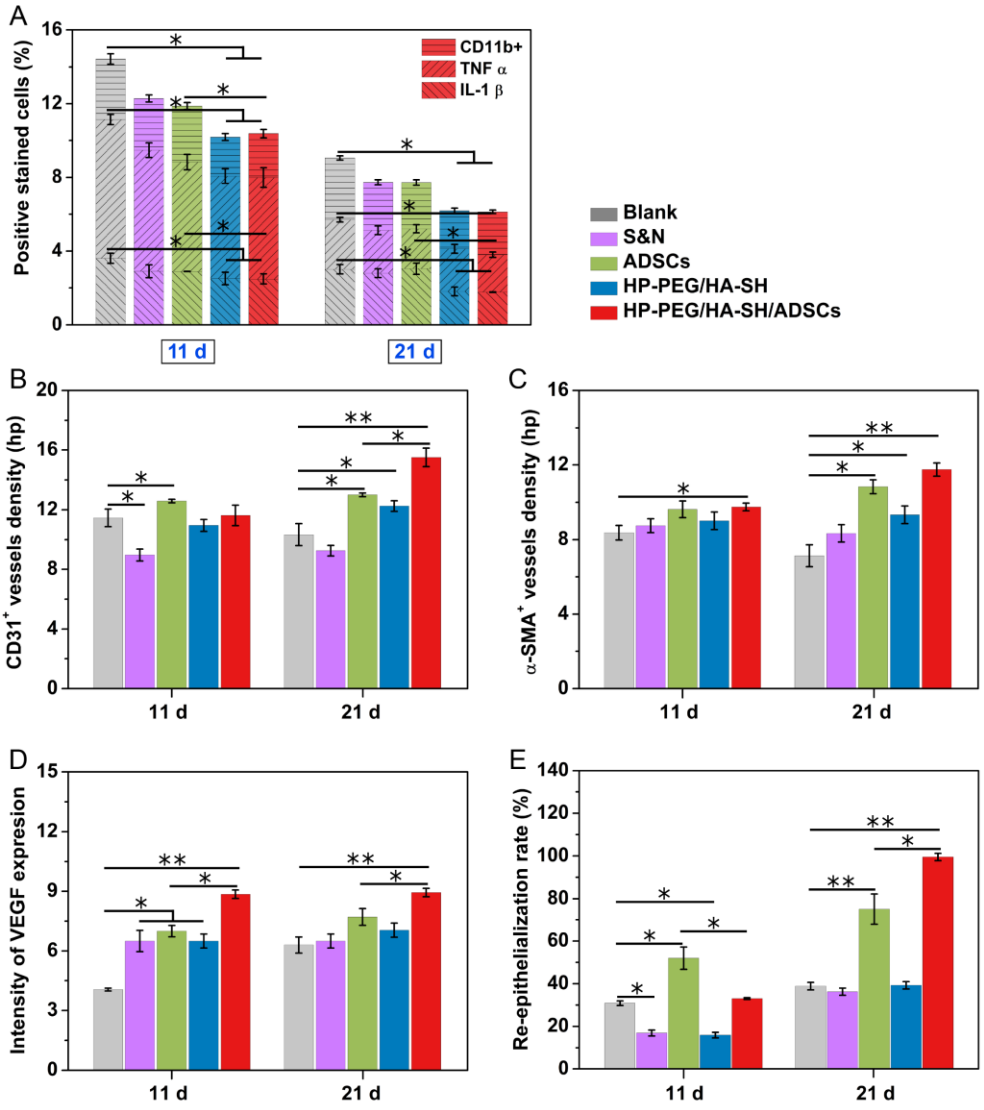

Figure 6. Quantitative analysis based on the immunohistochemical staining slides. A, Quantification analysis of the positive stained inflammatory cytokines which indicate total cellular infiltration in the wound areas as well as immune response in the surrounding tissue. Less secretion of inflammatory factors is observed in injectable HP-PEG/HA-SH/ADSCs hydrogel treated wounds. B and C, Quantifications analysis of blood vessels based on CD31 and α-SMA positive stained vasculature. CD31 is located on the surface of endothelial cells; α-SMA is localized on smooth muscle cells; both are known markers for vascular networks. The injectable hydrogels treated group exhibits significantly higher vessel density than no-treatment group at 11 and 21 days post-wounding. D, Intensity of VEGF expression in each experimental group. More secretion of VEGF is seen in HP-PEG/HA-SH/ADSCs hydrogel treated wounds. E, Quantification analysis of re-epithelialization rate at days 11 and 21 post-wounding. There is a much faster re-epithelialization rate in injectable HP-PEG/HA-SH/ADSCs hydrogel than that in no-treatment group. *, $p<0.05$; **, $p<0.01$.

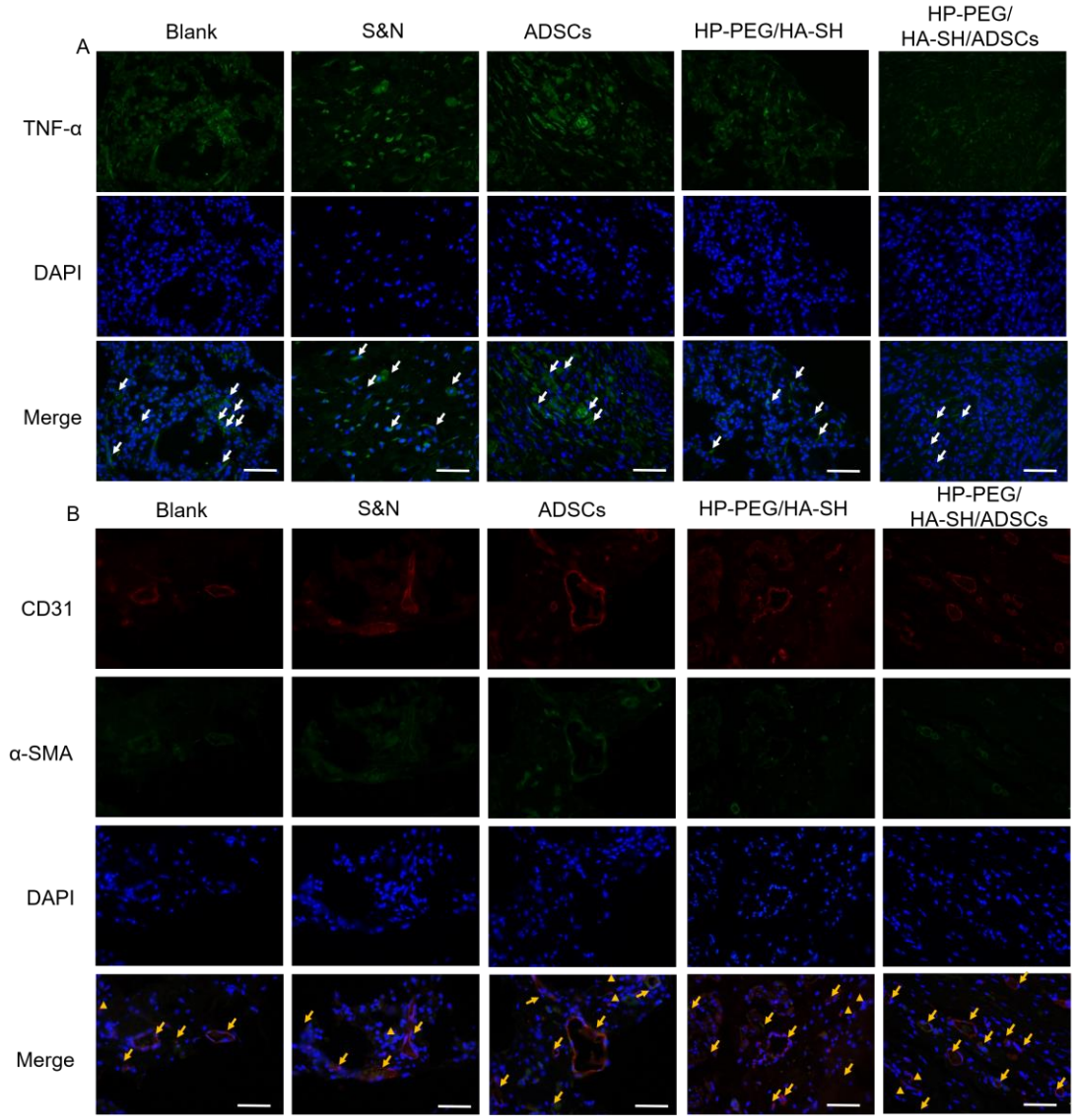

Figure 7. Immunofluorescent staining of wound sections in diabetic wound tissues. A, Representative immunofluorescent images of tissue sections at 11 days post-wounding for TNF-α (green) and DAPI staining for nuclei (blue). B, Representative immunofluorescent images of tissue sections for CD31 (red), α-SMA (green), and DAPI (for cell nuclei, blue) stained images (21 days post-wounding). Yellow triangles represent CD31+/α-SMA- vessels, and yellow arrows represent CD31+/α-SMA+ vessels. Scale bar: 100 μm.